INTERNATIONAL JOURNAL FOR NUMERICAL METHODS IN FLUIDS, VOL. 23, 431–444 (1996)

A VORTICITY–STREAMFUNCTION FORMULATION FOR STEADY INCOMPRESSIBLE TWO-DIMENSIONAL FLOWS

P. CHAVIAROPOULOS

Centre for Renewable Energy Sources, Wind Energy Department, 19 km Marathonos Ave., 19009 Pikermi, Attiki, Greece

AND

K. GIANNAKOGLOU*

Laboratory of Thermal Turbomachines, National Technical University of Athens, PO Box 64069, Athens 157 10, Greece

SUMMARY

A vorticity–streamfunction formulation for incompressible planar viscous flows is presented. The standard kinematic field equations are discretized using centred finite difference schemes and solved in a coupled way via a Newton-like linearization scheme. The linearized system of partial differential equations is handled through the restarting linear GMRES algorithm, preconditioned by means of an incomplete LU approximate factorization. The proposed solution technique constitutes a fast and robust algorithm for treating laminar flows at high Reynolds numbers. The pressure field is obtained at a subsequent step by solving a convection–diffusion equation in terms of the stagnation pressure, which presents certain advantages compared with the widely used static pressure Poisson equation. Results are shown for a wide variety of applications including internal and external flows.

KEY WORDS: laminar flows; incompressible flows; vorticity–streamfunction formulation; Krylov subspace methods; preconditioning

INTRODUCTION

During the last decades several techniques have been developed for the numerical integration of the laminar incompressible Navier–Stokes equations. Established formulations include those based on primitive variables and those using appropriate transformations such as the vorticity–streamfunction transformation, which is by far the one most commonly used.

A method based on the solution of primitive flow variables provides a better insight into the physical conservation laws and their boundary conditions. Two- and three-dimensional flows may be handled equally well with similar algorithms. Turbulence models, when needed, are straightforward to implement. On the other hand, primitive variable formulations for incompressible flows lack a physically meaningful pressure equation. A Poisson pressure equation is often used[1] by applying the divergence operator on the momentum equation. If the pressure equation is formed directly on the discretized equations, the resulting system consisting of the pressure Poisson equation and the

* Corresponding author.

CCC 0271–2091/96/050431–14

Received May 1995
Revised January 1996

momentum equations is equivalent to the original system of flow equations. A pressure correction term, which is related directly to the velocity field,[2] offers an alternative possibility. This term, premultiplied by a linearized operator, appears finally in the continuity equation, providing the pressure equation that must be solved. The choice of the operator characterizes the different pressure correction techniques. When only diagonal entries are retained in the operator, the method is usually referred to as artificial compressibility.[3] Primitive variable formulations lead to velocity–pressure decoupling problems, which appear when collocated discretization schemes are employed. Staggering techniques[4] offer a remedy but increase the complexity of programming. An alternative way to avoid decoupling problems is by spreading the pressure finite difference stencil[5] or by choosing different interpolation levels for the velocity and the pressure, especially in finite solvers.[6] In all these techniques, however, the accuracy of the final solution is affected to some extent.

The vorticity–streamfunction (Ψ–ω) formulation offers a convenient alternative to primitive variable formulations for representing the kinematic nature of the incompressible Navier–Stokes equations. A first advantage of this formulation is related to the automatic satisfaction of the continuity equation due to the use of the streamfunction, while the absence of a pressure gradient term in the vorticity equation eliminates problems related to the velocity–pressure decoupling. On the other hand, the closed form of the resulting system of equations makes it amenable to fast numerical integration using appropriate iterative or direct solvers. The above two reasons make the Ψ–ω formulation very attractive for the accurate solution of high-Reynolds-number planar or axisymmetric Navier–Stokes equations. However, a few drawbacks still affect the Ψ–ω formulations. Among them, the most important seems to be the difficulty in extending the method to 3D and to the transonic regime. Many improvements have been contributed by other researchers in order to overcome these shortcomings. As an example, Davis *et al.*[7] extended the method to three-dimensional viscous and inviscid flows, while Xu *et al.*[8] offered solutions for the double-root problem when calculating density in transonic flows. However, three-dimensional or compressible flow problems are beyond the scope of this work. An additional drawback is the necessity to use approximate and iterative vorticity boundary conditions along solid walls. Habashi *et al.*[9] improved the stability of both the scheme and the boundary condition formulation using a finite element analysis.

In Ψ–ω formulations the kinematic field is determined independently from the pressure field. The latter, if needed, is provided at a subsequent step by solving a Poisson-type equation similar to the one employed in primitive variable formulations. The proper specification of pressure boundary conditions is essential when a pressure Poisson equation is used. The role of pressure boundary conditions is discussed in detail by Gresho and Sani.[10]

The present work deals with the numerical integration of the laminar incompressible 2D Navier–Stokes equations using the Ψ–ω formulation. The governing equations are discretized using second-order-accurate finite difference/finite volume schemes and body-fitted curvilinear co-ordinates. In an effort to add new information to the voluminous work published on Ψ–ω techniques, the paper focuses on three topics which, in the authors's opinion, are still open.

(a) The implementation of a vorticity boundary condition in non-regular meshes which is compatible with the finite volume scheme in use.
(b) The accurate solution of the pressure field using the stagnation instead of the static pressure as the dependent variable. The stagnation pressure satisfies a convection–diffusion equation whose right- hand side (RHS) and boundary conditions are directly related to the computed vorticity field.
(c) The formulation of a fast and robust iterative scheme for the solution of the governing equations. This scheme is based on the restarting linear GMRES[11] algorithm, preconditioned

by scalar matrices which result from the incomplete LU decomposition (modified strongly implicit procedure (MSIP)[12] algorithm) of the Laplacian and convection–diffusion operators.

The accuracy and convergence properties of the proposed solver are investigated in representative internal and external flow computations for a wide range of Reynolds numbers.

GOVERNING EQUATIONS

When streamfunction and vorticity are introduced in the flow equations for incompressible two-dimensional flows, the resulting set of kinematic equations reads

$$\mathbf{V} = \nabla \times \boldsymbol{\Psi} = \nabla\boldsymbol{\Psi} \times \mathbf{N}, \qquad \boldsymbol{\Psi} = \mathbf{N}\Psi, \tag{1}$$

$$-\nabla^2\boldsymbol{\Psi} = \boldsymbol{\omega}, \qquad \boldsymbol{\omega} = \mathbf{N}\omega = \nabla \times \mathbf{V}, \tag{2}$$

$$\frac{\partial \boldsymbol{\omega}}{\partial t} + \mathbf{V}\cdot\nabla\boldsymbol{\omega} - \frac{1}{Re}\nabla^2\boldsymbol{\omega} = 0, \tag{3}$$

where $\mathbf{N}$ is the unit vector normal to the flow plane. All equations are assumed to be non-dimensional, having been normalized by a suitable combination of a characteristic velocity and a characteristic length. The introduction of the streamfunction satisfies the continuity equation automatically, while the vorticity definition provides a linear Poisson equation for the streamfunction. Equation (3) which results from the momentum equations is a non-linear one, the Reynolds number being a measure of its non- linearity. It is worth noting that equations (1)–(3) are independent of the pressure field, which may be determined in a subsequent step once the kinematic field is known.

It is a common practice to determine the pressure field from a Poisson equation resulting from the divergence of the momentum equation. This equation becomes

$$-\frac{1}{\rho}\nabla^2 p = \nabla\cdot\left(\frac{\partial \mathbf{V}}{\partial t} + \mathbf{V}\cdot\nabla\mathbf{V}\right),$$

where ρ is the constant fluid density and is solved by applying Neumann boundary conditions along the solid walls. For a given velocity field, local inaccuracies in calculating the second-order RHS derivatives may limit the convergence rate of this equation unless the integral constraint (Green's theorem) is globally satisfied.

In order to circumvent the above problem, a new pressure formulation based on the stagnation pressure transport equation is proposed. The latter is deduced from the combination of the inner product of the momentum equation with the velocity vector and the divergence of the momentum equation. The resulting convection–diffusion equation in terms of the stagnation pressure p_t, or rather the ratio p_t/ρ, reads

$$\frac{1}{2}\frac{\partial(V^2)}{\partial t} + \mathbf{V}\cdot\nabla\left(\frac{p_t}{\rho}\right) - \frac{1}{Re}\nabla^2\left(\frac{p_t}{\rho}\right) = -\frac{1}{Re}\omega^2, \tag{4}$$

where, by definition, the stagnation pressure p_t is

$$p_t = p + \tfrac{1}{2}\rho V^2. \tag{5}$$

The RHS term in (4) is computed easily and accurately since it merely depends on the vorticity, being one of the solution variables in the present formulation. Equations (3) and (4) may be numerically integrated using the same algorithm. Since equation (4) is solved for the stagnation pressure, an accurate prediction of flow losses is ensured.

Equations (1)–(3) constitute a closed system of equations governing the kinematic field. Once the kinematic field is known, equation (4) is a linear partial differential equation (PDE) which may provide the stagnation pressure field. Then the static pressure can be deduced from (5).

BOUNDARY CONDITIONS

The elliptic Ψ-equation requires boundary conditions along the complete boundary of the computational domain. In internal aerodynamics Ψ is set equal to zero on the lower wall and equal to the total mass influx on the upper wall. In external aerodynamics Ψ is set to zero on the body, independently of the incidence angle, while Neumann boundary conditions are imposed along the inflow boundary. In both internal and external flows, fully developed flow conditions are imposed at the exit boundary.

The boundary conditions for ω are of the Dirichlet type along the inflow and solid boundaries. The wall vorticity values are determined from (2) in a way which is consistent with the discretization scheme employed. Further details will be given below. Fully developed vorticity conditions are imposed at the outflow boundary.

A Neumann condition for the stagnation pressure is provided by projecting the momentum equation in the direction normal to the boundary. Along the solid walls the no-slip condition simplifies the aforementioned equation to

$$\frac{\partial(p_t/\rho)}{\partial n} = \frac{1}{Re}\frac{\partial \omega}{\partial s}, \tag{6}$$

where n and s are the normal and tangential directions to the wall. Unlike the commonly used static pressure Neumann boundary condition, the one used for the total pressure is directly related to the first derivative of the solution variable ω, providing similar benefits in accuracy to those previously quoted.

An alternative way to obtain a stagnation pressure boundary condition is by projecting the momentum equation in the direction tangential to the wall. This results in the expression

$$\frac{\partial(p_t/\rho)}{\partial s} = -\frac{1}{Re}\frac{\partial \omega}{\partial n}, \tag{7}$$

which, then integrated along the solid walls, provides Dirichlet boundary conditions for p_t. Equation (7) expresses the near-wall velocity profile curvature $(\partial\omega/\partial n)$ in terms of the pressure derivative along the wall. The present method utilizes equation (6) instead of equation (7) as a boundary condition for the stagnation pressure field.

NUMERICAL PROCEDURE

Co-ordinate transformation

To increase the accuracy and flexibility of the computational method, a body- fitted co-ordinate transformation is used in order to map the physical Cartesian plane (x, y) onto a transformed curvilinear one. In the transformed domain the Laplacian operator takes the form

$$\nabla^2(\,) = \frac{1}{J}\frac{\partial}{\partial u^i}\left(Jg^{ij}\frac{\partial}{\partial u^j}(\,)\right) \quad (i,j = 1,2), \tag{8}$$

where

$$\mathbf{g}_i = \frac{\partial \mathbf{r}}{\partial u^i}, \qquad \mathbf{g}^i = \nabla u^i, \qquad g_{ij} = \mathbf{g}_i \cdot \mathbf{g}_j, \qquad g^{ij} = \mathbf{g}^i \cdot \mathbf{g}^j$$

are the covariant and contravariant orthonormal vector bases and metrics respectively and

$$J = |\mathbf{g}_1 \times \mathbf{g}_2| = [\det(g_{ij})]^{1/2}$$

is the Jacobian of the transformation.

The convection operator yields

$$\mathbf{V} \cdot \nabla( ) = V^i \frac{\partial( )}{\partial u^i} \quad (i = 1, 2), \tag{9}$$

where V^i are the contravariant velocity components related to the streamfunction derivatives through (1), namely

$$V^i = \epsilon^{ij} \frac{1}{J} \frac{\partial \Psi}{\partial u^j}, \tag{10}$$

with ε^{ij} the permutation tensor.

Discretization

The governing equations are discretized using centred finite difference/finite volume schemes. Assuming that $\Delta u^i = 1$ in the discrete computational plane, the Laplacian operator is discretized as

$$\nabla^2( ) = \frac{1}{J} \vec{\delta}_i \left(J g^{ij} \vec{\delta}_j( ) \right)$$

$$= \frac{1}{J} \{ [JU^1( )]_{fu^1} - [JU^1( )]_{bu^1} + [JU^2( )]_{fu^2} - [JU^2( )]_{bu^2} \}, \tag{11}$$

$$U^i( ) = g^{ij} \bar{\delta}_j( ), \tag{12}$$

where $\overleftarrow{\delta}_i$, $\vec{\delta}_i$ and $\bar{\delta}_i$ are respectively the backward, forward and centred derivative operators in the direction u^i. Indices fu^1, bu^1, etc. are used to address mid-node locations (f: forward, b: backward in directions u^1, u^2) and $JU^i( )$ are the 'diffusive' fluxes. These fluxes are calculated at the mid-nodes of the grid using local metrics.

The convection operator is discretized in non-conservative form over the grid nodes using central differencing, namely

$$\mathbf{V} \cdot \nabla( ) = V^i \bar{\delta}_i( ). \tag{13}$$

The Neumann boundary conditions are incorporated implicitly in the finite volume scheme by suitable modifications of the coefficients Jg^{ij} appearing in the discrete Laplacian operator, as described by Holst.[13]

Discrete form of vorticity boundary condition on solid walls

Special attention is paid to the implementation of a vorticity boundary condition which maintains the compatibility with the finite volume discretization scheme and is valid for arbitrary, not necessarily regular, meshes. The vorticity values on the solid walls result from (2), which is

discretized in the half-cell adjacent to the solid boundary. Let $u^2 = u^2_{\min}$ stand for a co-ordinate line which corresponds to a solid boundary (subscript 'w'). Along this line the no-slip condition implies that

$$\frac{\partial \Psi}{\partial u^i}\Big|_w = 0 \quad (i = 1, 2)$$

and consequently the fluxes $JU^i(\Psi)$ $(i = 1, 2)$ vanish at any node or mid-node along the line $u^2 = u^2_{\min}$.

According to the discretization scheme (11) and the aforementioned remarks, the Ψ-fluxes at the mid-nodes around any boundary node yield

$$[JU^1(\Psi)]_{fu^1} = [JU^1(\Psi)]_{bu^1} = 0,$$
$$[JU^2(\Psi)_{fu^2} + [JU^2(\Psi)]_{bu^2} = 2[JU^2(\Psi)_w] = 0.$$

The latter results by assuming that the fluxes are linearly distributed within a grid cell. This expression is used to eliminate the contribution of the mid-node (bu^2) lying outside the flow domain. As a consequence, the discrete form of (2) reads

$$\omega_w = -(\nabla^2\Psi)_w = -\frac{2}{J_w}[JU^2(\Psi)]_{fu^2}, \tag{14}$$

constituting a Dirichlet boundary condition on ω. Similar expressions are valid along the remaining solid walls. When a general non- orthogonal grid is used, the wall vorticity at each boundary node is linearly related to the streamfunction values of the surrounding six half-stencil nodes. The approach can be considered as an extension of existing first-order- accurate vorticity boundary conditions (see discussion in References 14 and 15) to non-regular meshes.

Numerical integration scheme

The numerical integration of the kinematic field equations (2) and (3) is obtained in a strongly coupled way by using a Newton iterative scheme. Let $f = \{\Psi, \omega\}^T$ stand for the array of dependent variables and R be the residual array which is expressed as

$$R^n = \begin{bmatrix} \nabla^2 & I \\ O & \mathbf{V}^n \cdot \nabla - (1/Re)\nabla^2 \end{bmatrix} f^n, \tag{15}$$

where the superscript n denotes the iteration level.

The Newton iteration step is formed as

$$R^{n+1} = R^n + \left(\frac{\partial R}{\partial f}\right)^n \Delta f = 0, \tag{16}$$

where

$$f^{n+1} = f^n + \Delta f. \tag{17}$$

The Jacobian matrix is given by

$$\left(\frac{\partial R}{\partial f}\right) = \begin{bmatrix} A_{11} & I \\ A_{21} & A_{22} \end{bmatrix} = \begin{bmatrix} \nabla^2 & I \\ \nabla \times (\,) \cdot \nabla\omega^n & I/\Delta t + \mathbf{V}^n \cdot \nabla - (1/Re)\nabla^2 \end{bmatrix}, \tag{18}$$

including the Laplacian operator A_{11}, the unsteady transport–diffusion operator A_{22} (where a first-order time discretization scheme has been useed, with Δt being the time step) and also the cross-operator A_{21} which results from the linearization of the convection part in (3) by taking also into account the definition (1).

The linearized system of equations (16) is left preconditioned by a matrix P, which is an approximation of the inverse of the Jacobian matrix, after excluding the cross-term A_{21} for the sake of simplicity. The simplification aims at avoiding block matrix inversion during the preconditioning. The preconditioner P reads

$$P^n \approx \left[\left(\frac{\partial R}{\partial f}\right)^n\right]^{-1} \approx \begin{bmatrix} A_{11}^{-1} & -A_{11}^{-1}A_{22}^{-1} \\ O & A_{22}^{-1} \end{bmatrix}. \tag{19}$$

In order to facilitate the preconditioning process, the diagonal block matrices in (18) are approximately factored using the MSIP[12] approximate factorization technique and P^n finally becomes

$$p^n = \begin{bmatrix} p_{11}^{-1} & -p_{11}^{-1}p_{22}^{-1} \\ O & p_{22}^{-1} \end{bmatrix}, \tag{20}$$

where P_{11} results from the incomplete LU decomposition of the Laplacian operator A_{21} and P_{22} from the incomplete LU decomposition of the unsteady convection–diffusion operator A_{22}. The left-preconditioned form of (16) is

$$R^* + D\Delta f = 0, \tag{21}$$

where

$$R^* = (PR)^n, \qquad D = [P(\partial R/\partial f)]^n.$$

Considering that $D \approx I$, equation (21) may provide the updated values of f using the approximation $\Delta f = -R^*$; this approach can be classified as a coupled MSIP solver which handles the Ψ–ω equations in a fully implicit, partially coupled way, taking into account the non-diagonal identity terms of the Jacobian matrix. In order to increase the convergence rate of the solver, the original form of the matrix D is retained and the system of equations (21) is solved using the restarting linear GMRES(m) algorithm.[11] It is worth mentioning that the streamfunction and vorticity boundary conditions are easily implemented in the restarting linear GMRES scheme owing to their linear form. The same basic numerical scheme is used by the authors in numerous CFD applications.[16,17]

A similar numerical integration technique is adopted for the computation of the stagnation pressure field through (4). However, because of the linear character of this equation, simpler schemes may be used without a noticeable deterioration in performance.

The inversion of P_{11} or P_{22} is a straightforward task requiring the invesion of an upper and a lower triangular matrix resulting from the incomplete LU decomposition of A_{11} or A_{22} respectively. A_{11} is only factored once, while A_{22} is factored during each Newton step since it depends on the current velocity field. The MSIP scheme (although heavy in terms of storage requirements) was preferred among others because of its robustness and good convergence properties. Previous attempts of the authors based on ADI approximate factorization schemes presented convergence difficulties. This was partially due to the pseudotime numerical term that ADI introduces inherently. This term is not desirable when factoring the Laplacian operator of the steady Ψ-equation. In its present form the algorithm is used for steady computations only. First-order time-accurate computation may also be performed once the linearized problem (16) is fully converged during each Newton step. However, to avoid error truncation in unsteady computations due to the linearization process, the time-derivative term must be retained within the residual expression of the ω-equation. Further discussion on the unsteady features of the presented algorithm is beyond the scope of this paper.

RESULTS AND DISCUSSION

The capabilities of the proposed method are first demonstrated on two well-documented incompressible Navier–Stokes cases, namely the square driven cavity[18] and the backward-facing step.[19] The driven cavity case is used for the investigation of the convergence properties of the iterative solver; in the same case a parametric study of the effect of the Krylov base dimension m of the restarting linear GMRES(m) scheme on the convergence behaviour is also carried out. In the backward-facing step case the accuracy of the prediction of the characteristic lengths of the recirculation zones is investigated.

The driven cavity problem is studied for three Reynolds numbers ($Re = 100$, 400 and 1000) on three different grids (21×21, 41×41 and 81×81 nodes). All grids are non-uniform and stretched close to the solid walls by means of a geometric progression rule; for the three aforementioned grids the distance of the first node off the wall is $3{\cdot}14 \times 10^{-2}$, $8{\cdot}73 \times 10^{-3}$ and $2{\cdot}8 \times 10^{-4}$ respectively, while the cavity height is unity.

The effect of the Krylov base m on convergence is studied in terms of the drop of the L^2-residual norm of the vorticity equation versus the number of equivalent LU iterations. The latter is defined as the product of the number of Newton iterations and the dimension of the Krylov space used. This is in fact a measure of the number of factorizations employed. It is worth noting that the vorticity and streamfunction equations present similar convergence properties and for this reason the residual of the first only is examined. Table I summarizes the results from the parametric study for seven values $m = 3$, 5, 8, 10, 15, 20 and 25. All runs were performed with a global time step $\Delta t = 1$; convergence, shown in terms of equivalent LU iterations, is assumed when the residual drops by eight orders of magnitude. The $Re = 1000$ case is not examined on the 21×21 grid since the grid is too coarse for this Reynolds number. For the opposite reason the study of the $Re = 100$ case on the 81×81 grid is also omitted. It is seen that for a given Reynolds number the optimum value of m increases with the size of the grid. On the other hand, for a given grid size the optimum value of m decreases as the Reynolds number increases. This behaviour is expected considering that m is a measure of the convergence depth within each time level where a linearized subproblem is solved. Thus, when the grid size increases, the linear subproblem becomes stiffer and consequently a larger m-value is more appropriate. When the Reynolds number increases, the non-linearity of the flow is more pronounced and a deeper convergence of the linear subproblem is needless; this is why smaller values of m seem to be more effective. Figure 1 illustrates the convergence history for the $Re = 1000$ case on the two finer grids using the optimum m-values as chosen from Table I. The streamfunction and vorticity residuals are plotted together in order to demonstrate the aforementioned similarity in their convergence behaviour. Figures 2 and 3 show the horizontal and vertical velocity component profiles along the vertical and horizontal centrelines of the square domain for the cases $Re = 400$ and 1000 respectively. In the $Re = 400$ case the 21×21 grid is insufficient, while the 41×41 and 81×81 grids provide almost identical results. In the $Re = 1000$ case the differences between the 41×41 and 81×81 grids are more visible and a grid-independent solution requires a finer grid.

The backward-facing step geometry and boundary conditions were obtained from Reference 19. Several runs were performed in the range of Reynolds numbers from 100 to 1000. It is known from theory and experiments that besides the primary recirculation zone, a secondary recirculation zone develops on the upper wall as the Reynolds number increases. A graphical representation of the characteristic lengths of the two recirculation zones is given in Figure 4. An 80×40 grid was used for the present calculations and the results obtained are compared with the experimental data and the numerical results of Reference 19. The evolution of the characteristic lengths x_1, x_2 and x_3 with the Reynolds number is shown in Figures 5(a)–5(c) respectively. It may be observed that the comparison with the experimental values is fairly good for low Reynolds numbers, while large discrepancies

Table I. Parametric study of effect of Krylov subspace dimension m on convergence. The required number of equivalent LU iterations for a residual drop of eight orders of magnitude is tabulated for the driven cavity problem

	21 × 21		41 × 41			81 × 81	
	$Re=100$	$Re=400$	$Re=100$	$Re=400$	$Re=1000$	$Re=400$	$Re=1000$
$m=3$	84	276	144	249	528	–	–
$m=5$	160	425	130	345	800	2745	3675
$m=8$	240	672	192	472	984	1592	2944
$m=10$	290	840	255	550	> 1000	1380	2450
$m=15$	420	> 1000	345	810	> 1000	1065	2115
$m=20$	580	> 1000	420	> 1000	> 1000	1040	2620
$m=25$	725	> 1000	525	> 1000	> 1000	1225	3200

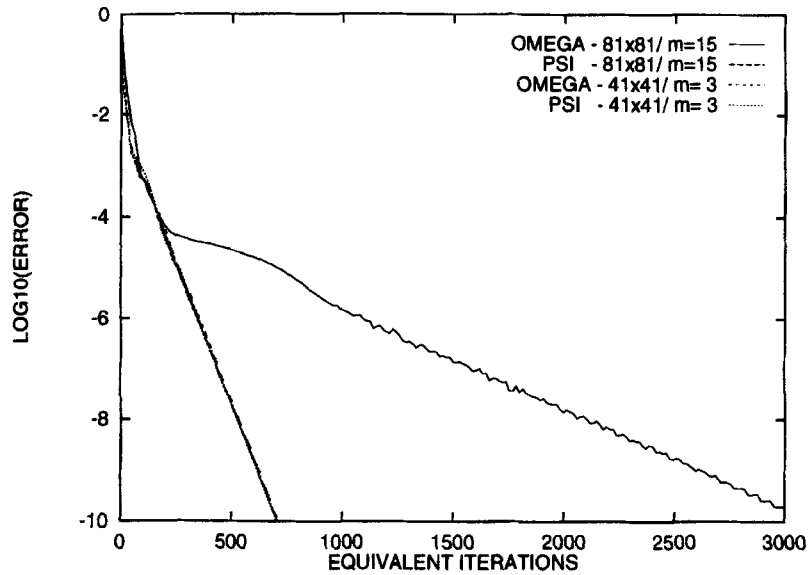

Figure 1. Convergence history of vorticity and streamfunction equations in driven cavity problem for $Re=1000$ on 41 × 41 and 81 × 81 grids

occur as the Reynolds number approaches 1000. This behaviour is expected, since in this Reynolds number range the flow lacks its steady two-dimensional character. Some more detailed comparisons of velocity and pressure field contours with numerical results obtained on unstructured grids may be found in Reference 20.

Two additional test cases are selected in order to investigate the performance of the method for higher Reynolds numbers. The first case concerns the development of the laminar boundary layer along a flat plate of uniform chord at Reynolds number (based on chord) equal to 5000. A 72 × 80 grid was generated for this computation, similar to that used by Mavriplis *et al.*[21] The grid spacing in the direction normal to the wall was performed using the logarithmic law, with the first interior node being at a 5×10^{-4} distance from the wall. The inlet flow plane was placed two chords upstream from the flat plate leading edge. The calculated velocity profiles tangential and normal to the wall as well as the shear stress profile are non-dimensionalized in terms of the laminar boundary layer

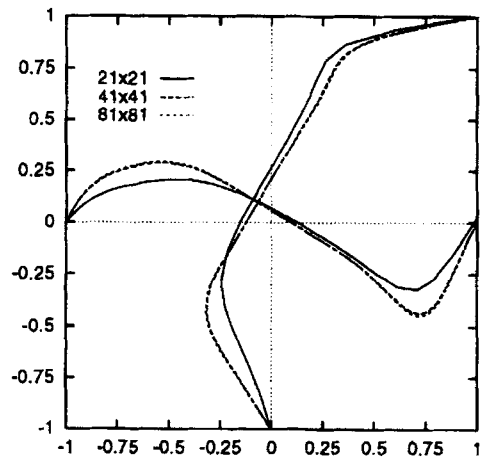

Figure 2. Horizontal and vertical velocity profiles along vertical and horizontal centrelines of cavity for $Re = 400$

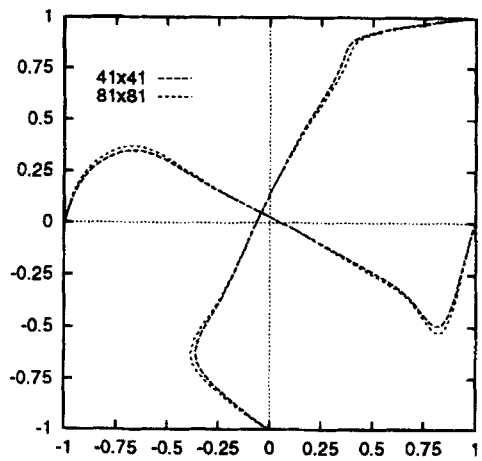

Figure 3. Horizontal and vertical velocity profiles along vertical and horizontal centrelines of cavity for $Re = 1000$

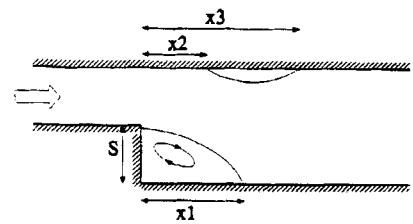

Figure 4. Recirculation zones in case of backward-facing step

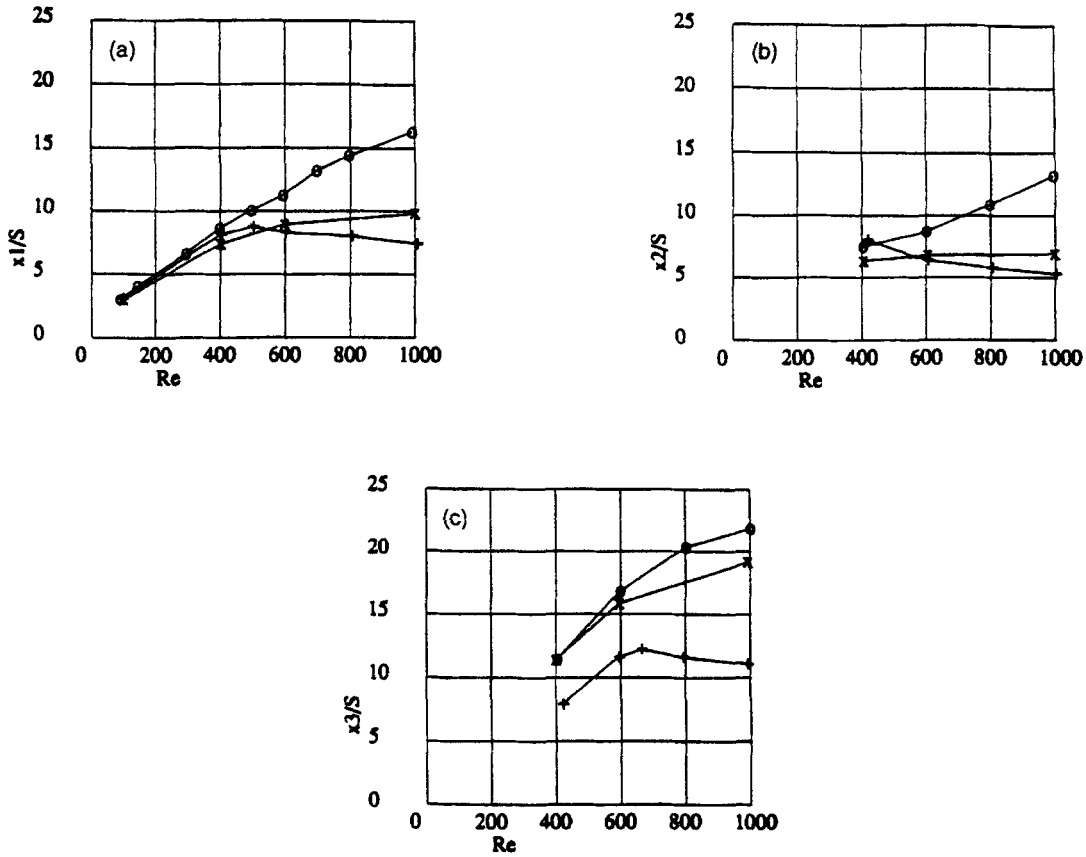

Figure 5. Evolution of characteristic lengths with Reynolds number: O, experiment; +, Reference 19; ×, present predictions

similarity laws and are compared with the Blasius solution in Figures 6–8. The comparison is performed at 30 per cent, 40 per cent, 50 per cent, 60 per cent and 70 per cent of the chord. The agreement between the calculated profiles and the semianalytical Blasius solution is very good, even at the 30 per cent and 70 per cent locations which are affected by the leading edge presence and the outflow boundary conditions respectively.

The last test case deals with the NACA 0012 isolated aerofoil at $Re = 5000$ and 0° incidence. At this Reynolds number, which is close to the limit of steady state behaviour, a small recirculation zone develops in the near-trailing edge region. A computation performed by Mavriplis *et al.*[21] for the corresponding compressible flow with $M_\infty = 0{\cdot}5$ estimates the separation point at approximately 82 per cent of the chord. For the incompressible case the separation point is expected to be further downstream. A 249 × 61 C-type grid with 165 nodes on the aerofoil was used for the present computation (Figure 8), with the minimum first-node distance from the profile being of the order of 5×10^{-4} of the chord. The cell aspect ratios in the wake region near the outflow boundary are of the order of 1000 : 1, making the computation particularly stiff. The computed C_p and C_f distributions along the profile are shown in Figures 9 and 10 respectively. From the C_f distribution (which is directly related to the vorticity on the wall) the separation point was predicted at 93·3 per cent of the chord. One may notice the sharp peak of the C_f curve in the near-leading edge region, which is usually underpredicted by any primitive variable solver. Since the vorticity field is directly related to

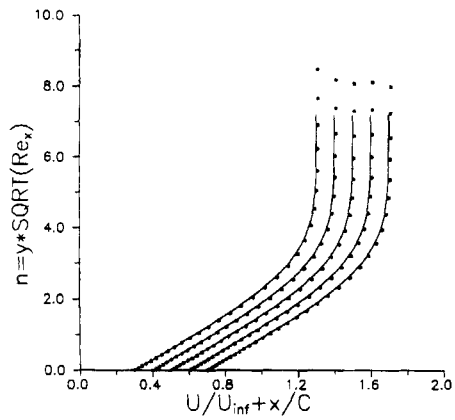

Figure 6. Comparison of predicted tangential velocity profiles (*) with Blasius solution (—). Flow along a flat plate

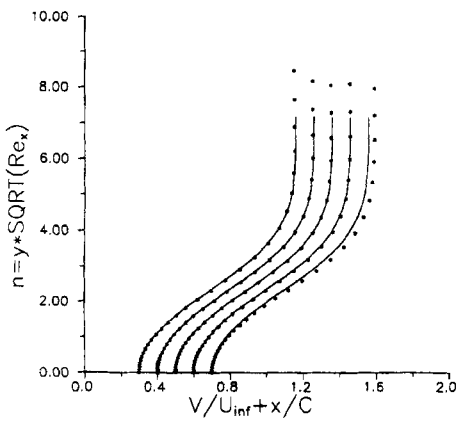

Figure 7. Comparison of predicted normal velocity profiles (*) with Blasius solution (—). Flow along a flat plate

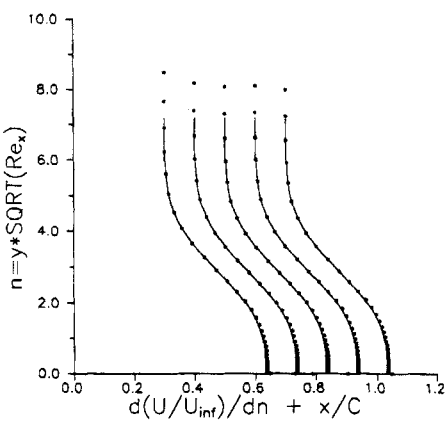

Figure 8. Comparison of predicted shear stress profiles (*) with Blasius solution (—). Flow along a flat plate

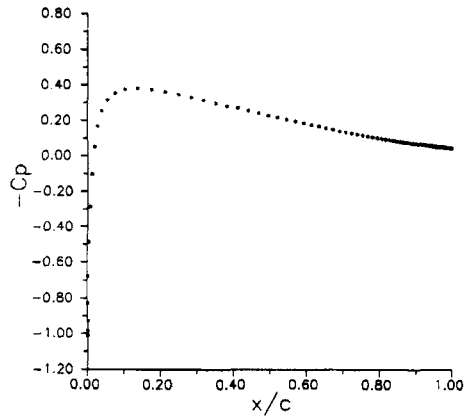

Figure 9. Predicted distribution of c_p. NACA 0012, $Re = 5000$

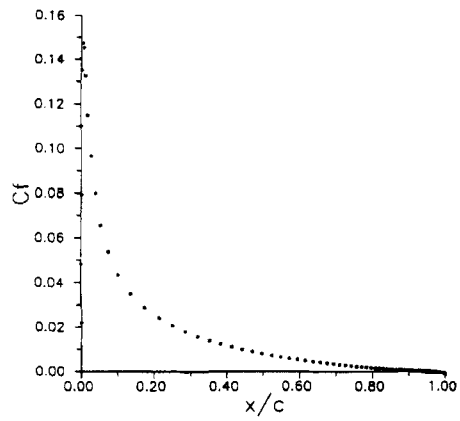

Figure 10. Predicted distribution of c_f. NACA 0012, $Re = 5000$

the stagnation pressure field (the ω^2 source term in (4) and the $\partial\omega/\partial s$ term appearing in the stagnation pressure boundary condition), an underprediction of the vorticity in the near-leading edge region may also affect the accuracy of the pressure coefficient computation.

In the last two problems optimum convergence was obtained by means of a Krylov subspace dimension equal to 15. In both cases convergence was assumed when the streamfunction and vorticity residuals had dropped by five orders of magnitude.

CONCLUSIONS

A formulation for modelling two-dimensional steady incompressible viscous flows was presented. This formulation is based on the coupled solution of the streamfunction and vorticity equations via a Newton-like linearization scheme. A preconditioned GMRES algorithm is used for handling the resulting system of partial differential equations. The vorticity wall boundary condition is treated implicitly in a consistent way with a finite volume discretization scheme which is used in the interior

of the computational domain. Once the correct kinematic field has been obtained, the pressure field is calculated through the numerical integration of a convection–diffusion equation in terms of the stagnation pressure.

The accuracy and robustness of the method are assessed through several computations, which were performed for a number of well-documented test cases and at various Reynolds numbers. It is demonstrated that the appropriate selection of the Krylov subspace dimension m is critical for the efficiency of the algorithm. In the cavity problem examined, the recommended values of m are in the range $m = 3$–15, depending upon the size of the mesh and the flow Reynolds number. The optimum value of m increases with the grid size and decreases with the Reynolds number.

REFERENCES

1. A. J. Chorin, 'Numerical solution of the Navier–Stokes equations', *Math. Comput.*, (1968).
2. V. S. Pratap and D. B. Spalding, 'Fluid flow and heat transfer in three-dimensional duct flows', *Int. J. Heat Mass Transfer*, **19**, 1183–1188 (1976).
3. D. Kwak, J. L. C. Chang, S. P. Shanks and S. R. Chakravarthy, 'A three-dimensional incompressible Navier–Stokes flow solver using primitive variables', *AIAA J.*, **24**, 390–396 (1986).
4. S. V. Patankar and D. B. Spalding, 'A calculation procedure for heat, mass and momentum transfer in three-dimensional parabolic flows', *Int. J. Heat Mass Transfer*, **15**, 1787–1806 (1972).
5. C. M. Rhie and W. L. Chow, 'Numerical study of the turbulent flow past an aerofoil with trailing edge separation', *AIAA J.*, **21**, 1525–1532 (1983).
6. P. Hood and C. Taylor, 'A numerical solution of the Navier–Stokes equations using the finite element technique', *Comput. Fluids*, **1**, 73–100 (1973).
7. R. L. Davis, J. E. Carter and M. Hafez, 'Three-dimensional viscous flow solutions with a vorticity–streamfunction formulation', *AIAA J.*, **27**, 892–900 (1989).
8. J. Z. Xu, W. Y. Ni and J. Y. Du, 'Numerical solution of streamfunction equations in transonic flows', *J. Turbomach. ASME*, **109**, 508–512 (1987).
9. W. G. Habashi, M. F. Peeters, G. Guevremont and M. M. Hafez, 'Finite- element solutions of the compressible Navier–Stokes equations', *AIAA J.*, **25**, 944–948 (1987).
10. P. M. Gresho and R. L. Sani, 'On pressure boundary conditions for the incompressible Navier–Stokes equations', *Int. j. numer. methods fluids*, **7**, 1111–1145 (1987).
11. Y. Saad and M. H. Schultz, 'GMRES: a generalized minimal residual algorithm for solving nonsymmetric linear systems', *SIAM J. Sci. Stat. Comput.*, **7**, 856–869 (1986).
12. M. Zedan and G. E. Schneider, 'A three-dimensional modified strongly implicit procedure for heat conduction', *AIAA J.*, **21**, 285– 303 (1983).
13. T. Holst, 'Numerical computation of transonic flow governed by the full potential equation', *VKI Lecture Series 1981-05*, 1985.
14. S. A. Orszag and M. Israeli, 'Numerical solution of viscous incompressible flows', *Ann. Rev. Fluid Mech.*, **6**, 281–318 (1974).
15. P. M. Gresho, 'Incompressible fluid dynamics: some fundamental formulation issues', *Ann. Rev. Fluid Mech.*, **23**, 413–453 (1991).
16. K. Giannakoglou, P. Chaviaropoulos and K. D. Papailiou, 'Acceleration of standard full-potential elliptic flow solvers using preconditioned generalized minimal residual techniques', in *Flows in Non-Rotating Turbomachinery Components*, ASME-FED Vol. 69, 1988.
17. P. Kiousis, P. Chaviaropoulos and K. D. Papailiou, 'Meridional flow calculation using advanced CFD techniques', *ASME Paper 92-GT-325*, 1992.
18. R. Peyret and D. T. Taylor, *Computational Methods for Fluid Flow*, Springer, New York, 1983.
19. B. F. Armaly, F. Durst, C. F. Pereira and B. Schonung, 'Experimental and theoretical investigation of backward-facing step flow', *J. Fluid Mech.*, **127**, 473–496 (1983).
20. P. Chaviaropoulos, K. Giannakoglou, N. Lymberopoulos and G. Simandirakis, 'CFD in internal aerodynamic problems—Part 2', *First Year Report, Project G52, AGARD/OTAN/PEP 90*, 1991.
21. D. J. Mavriplis, A. Jameson and L. Martinelli, 'Multigrid solution of the Navier–Stokes equations on triangular meshes', *NASA Contractor Rep. 181786, ICASE Rep. 89-11*, 1989.